Synthesis, substitiuent effects, optical properties, and crystal structures of substituted platinum (II) biphenyl bipyridine complexes

SYNTHESIS, SUBSTITIUENT EFFECTS, OPTICAL PROPERTIES, AND CRYSTAL STRUCTURES OF SUBSTITUTED PLATINUM (II) BIPHENYL BIPYRIDINE COMPLEXES

A Thesis by

Ali Jehan

Bachelor of Science, Wichita State University, 2010

Submitted to the Department of Chemistry and Biochemistry
and the faculty of the Graduate School of
Wichita State University
in partial fulfillment of
the requirements for the degree of
Master of Science

July 2024

SYNTHESIS, SUBSTITIUENT EFFECTS, OPTICAL PROPERTIES, AND CRYSTAL STRUCTURES OF SUBSTITUTED PLATINUM (II) BIPHENYL BIPYRIDINE COMPLEXES

The following faculty members have examined the final copy of this thesis for form and content and recommend that it be accepted in partial fulfillment of the requirement for the degree of Master of Science with a major in Chemistry.

Paul Rillema, Committee Chair

Douglas English, Committee Member

David Eichhorn, Committee Member

Ramazan Asmatulu, Committee Member

DEDICATION

I dedicate this thesis to my father, Dr. Sayed Jehan. I wish he was around to see I didn't give up. A truly great man and philanthropist. Rest in peace.

“The important thing is to never stop questioning (or learning).” – Albert Einstein

ACKNOWLEDGEMENTS

I would like to thank the Department of Chemistry and Biochemistry of Wichita State University for giving me the opportunity to pursue a degree in both undergraduate and graduate studies. I especially my mentor and boss, Dr. Paul Rillema, for letting me work in his lab and for all the help he has given me over the years. I also thank Dr. Stan Stoyanov for theoretical calculations and Dr. Curtis Moore for X-Ray structure determinations.

ABSTRACT

A series of platinum(II) biphenyl 2,2'-bipyridine complexes containing electron-donating and electron-withdrawing moieties on the 4 and 4' positions of the bipyridine ligand exhibit emission from excited states in the 600 nm region of the spectrum upon excitation in the metal-to-ligand charge transfer transition (MLCT) absorption band located near 450 nm. These complexes are distorted from planarity based on both single crystal structure determinations and density functional theory (DFT) calculations of isolated molecules in acetonitrile. The DFT also reveals the geometry of the lowest-lying triplet state (LLTS) of each complex that is important for emission behavior. The LLTS are assigned based on the electron spin density distributions and correlated with the singlet excited states to understand the mechanism of electronic excitation and relaxation. Time-dependent DFT calculations are performed to compute the singlet excited state energies of these complexes so as to help interpret their UV-visible absorption spectra. Computational and experimental results, including absorption and emission energy maxima, electrochemical reduction potentials, LLTS, singlet excited states, lowest unoccupied molecular orbital (LUMO) and highest occupied molecular orbital (HOMO) energies, and exhibit linear correlations with the Hammett constants for para-substituents (σ_p). These correlations are employed to screen complexes that have not yet been synthesized. The correlation analysis indicates that electronic structure and the HOMO-LUMO energies, in Pt(II) complexes can be effectively controlled using electron-donating and electron-withdrawing moieties covalently bonded to the ligands. The information presented in this thesis provides analysis and better understanding of the fundamental electronic behavior of these complexes.

PREFACE

The platinum complexes of the form Pt(II)(bph)(bpy-x), where x are varying substituents, absorb light in the visible region and undergo emission at a lower energy (red shift). Our main goal was to analyze the regions of absorption and emission to determine if the compounds could be of use in light harvesting, or solar energy conversion. These particular compounds are of interest because they absorb light strongly in the visible range (high molar coefficients), Ɛ. Because of this property, in theory, it could be possible to capture energy in the form of light to be used as energy, where the molecules are excited, give off energy, and return to the ground state. A sort of light-cycling energy collection would be the end goal.

TABLE OF CONTENTS

Chapter Page

1. INTRODUCTION 1

2. SYNTHESIS OF COMPOUNDS 5
   2.1 Starting materials and instrumentation 5
   2.2 Synthesis of main precursor – $Pt[(bph)(Et_2S)]_2$ 6
   2.3 Synthesis of platinum compounds with various ligands having substituents in the 4,4' positions of the 2,2,-bipyridine ligand 9

3. CRYSTAL STRUCTURES AND DATA OF PLATINUM(II) BIPHENYL COMPLEXES..... 13
   3.1 Crystal data of $PtCl_2(Et_2S)_2$ and $[Pt(bph)(Et_2S)]_2$ 14
   3.2 Crystal structure data of Pt(bph)(4,4'-Me_2bpy), Pt(bph)(4,4'-Br_2bpy) and Pt(bph)(4,4'-$(COOC_2H_5)_2$bpy 16

4. ELECTRONIC PROPERTIES OF COMPOUNDS 21
   4.1 Beer's Law Studies.. 21
   4.2 UV/Visible Absorption 22
   4.3 Emission 24
   4.4 Electrochemistry 25

5. FREE ENERGY CORRELATIONS 27
   5.1 Absorption and Emission 27
   5.2 Electrochemistry 29
   5.3 Energy Gap Control 30

6. SUMMARY AND CONCLUSION 32

REFERENCES 34

APPENDICES 37

A. SOLVENT DEPENDENCY (SOLVATOCHROISM) OF COMPOUNDS 38

B. ALI JEHAN'S CO-AUTHORED POSTERS AND PUBLICATIONS 40

LIST OF TABLES

Table Page

3.1 Crystal data of $PtCl_2(Et_2S)_2$ and $[Pt(bph)(Et_2S)]_2$…… 15

3.2 Crystal Structure Data of Pt(bph)(4,4'-Me_2bpy), Pt(bph)(4,4'-Br_2bpy) and Pt(bph)(4,4'-$(COOC_2H_5)_2$bpy)…….. 16

3.3 Selected Bond Lengths (Å), Bond Angles (°) and Torsion Angles (°) Measured Using X-ray crystallography…… 19

4.1 Compounds and their absorption maxima and molar extinction coefficients …….. 23

4.2 Experimental Emission Results 25

4.3 Electrochemical Reduction Potentials ($E_{1/2}$) of Pt(bph)(4,4'-X_2bpy) Complexes 26

LIST OF FIGURES

Figure Page

1.1: Hammett Sigma Function 2

1.2: Jablonski Diagram 4

.

2.1: Removal of bromines from dibromobenzene to form a dianion 6

2.2: Synthesis of $PtCl_2(SEt_2)$ 7

2.3: Synthesis of $Pt_2(SEt_2)_2(bph)_2$ 8

2.4: Schematic of forming derivatives of Pt(bph)(4,4'-X_2bpy)
(X = H, CH_3, Br_2, NH_2, Ph, EtCOO) 9

3.1: Diagrams of $PtCl_2(Et_2S)_2$ and $[Pt(bph)(Et_2S)]_2$ starting compounds along
with their calculated crystal structures 14

3.2: Crystal structures of Pt(bph)(4,4'-Me_2bpy), Pt(bph)(4,4'-Br_2bpy)
and Pt(bph)(4,4'-$(COOC_5H_5)_2$bpy) 16

3.3: Crystal structures of Pt(bph)(4,4'-Me_2bpy), Pt(bph)(4,4'-H_2bpy) Pt(bph)(4,4'-Br_2bpy) and
Pt(bph)(4,4'-$(COOC_2H_5)_2$bpy) showing their X configuration in the solid state 20

4.1: Absorbance changes vs concentration for Pt(bph)(4,4'-CH_3-bpy) 21

4.2: Beer's law plot of absorbance vs. concentration for Pt(bph)(4,4'-Me_2-bpy) 22

4.3: Experimental Absorption of Pt(bph)(4,4'-X_2bpy) 23

4.4: Experimental emission spectra of Pt(bph)(4,4'-X_2bpy) 24

4.5: Differential pulse voltammograms of Pt(bph)(4,4'-X_2bpy) 26

5.1: Experimental UV-Vis Absorption and Calculated ^{1}MLLCT State Energies *vs* σ_p
(a), Experimental Emission and Calculated LLTS Energies *vs* σ_p
(b), Experimental emission lifetime *vs* σ_p (c), and Electrochemical reduction
potential $E_{1/2red}$ and E_{LUMO} *vs* σ_p (d) for the Pt(bph)(4,4'-X_2bpy) complexes 28

LIST OF FIGURES (continued)

Figure Page

5.2: Calculated $E_{LUMO} - E_{HOMO}$ energy gap *vs* σ_p for Pt(bph)(4,4'-X_2bpy)..... 30

A.1: Absorption of Pt(bph)(4,4'-Me_2-bpy) in various solvents 38

A.2: Scheme illustrating MLCT energy changes based on solvent polarity 39

LIST OF ABBREVIATIONS

AN	Acetonitrile
bph	Biphenyl
bpy	Bipyridine
DFT	Density Functional Theory
HOMO	Highest Occupied Molecular Orbital
LLCT	Ligand to Ligand Charge Transfer
LLTS	Lowest Lying Triplet State
LUMO	Lowest Unoccupied Molecular Orbital
MLCT	Metal to Ligand Charge Transfer
NMR	Nuclear Magnetic Resonance
LDA	Lithium Diisopropylamine
Me	Methyl
nm	Nanometers
N-BuLi	N-butyl lithium
Pt	Platinum
TDDFT	Time Dependent Density Functional Theory
UV	Ultraviolet

LIST OF SYMBOLS

A	Absorbance
c	Concentration
cm	Centimeters
σ_p	Hammett sigma para function
σ_m	Hammett sigma meta function
K	Kelvin
Ɛ	Molar extinction coefficient
M	Moles
nm	Nanometers
λ	Wavelength
µ	Micro
m	Meters

CHAPTER 1

INTRODUCTION

Our research group has been involved in the design of solar energy photocatalysts which absorb light in the visible region of the solar energy spectrum. The photocatalyst are coordination complexes [1,2] containing a metal center and an attached heterocyclic bidentate ligand. Upon absorption of light, an electron is transferred from the metal center to the heterocyclic ligand in a process referred to as metal to ligand transfer (MLCT). The electron transfers from the singlet excited state to a triplet excited prior to its return to the ground state in a process labeled emission which is slow enough for capture by another substrate such as methyl viologen[3,4]. The electronic processes are outlined in a Jablonski diagram in Figure 1.2.

This thesis reports the changes in electronic properties of a series of platinum(II) heterocyclic ligand complexes by altering the electronic density of the metal center using electronic donating/withdrawing substituents attached to the 4,4' positions of the 2,2'-bypyridine ligand. The substituents used in the study were NH_2, CH_3, H, C_6H_5, Br and $CO_2CH_2CH_3$ with Hammett sigma (σ_P) values of -0.66, -0.17, 0.10, 0.23, and 0.45, respectively, where negative values represent electron donors and positive values represent electron withdrawers which were determined experimentally based on the ionization constants of disubstituted benzoic acid[5,6].

Figure 1.1 shows the basis of the Hammett Sigma function. It is based off the ionization of benzoic acid. When the acid loses or gives up a proton, it has more electron density around the benzene ring. It gives an idea of how different substituents would effect the ionization, and σ_P, or Hammett Sigma values are based off this concept. Even though there is no acid or

ionization occurring and a bipyridine is involved instead of a benzene in the complexes of this study, the concept can still be applied, as both involve the aromatic rings gaining electron density. The results will show that this approximation to determine substituent effects show a very good relationship/correlation.

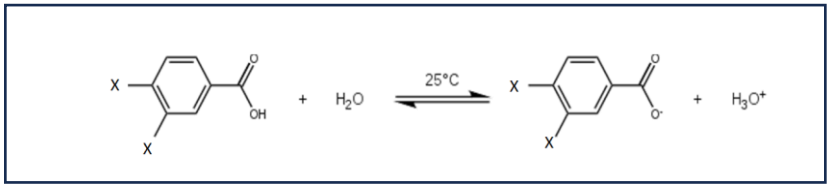

Figure 1.1 Hammett Sigma Function

By way of background, square planar platinum(II) complexes containing bidentate biphenyl and bidentate bipyridine chelating ligands are attractive emitters[7-9] with promising applications in optoelectronic devices[10], chemosensory materials[11] and catalysis[12]. The complexes display rich emission properties both in solution[7-9,13] and in the solid state[10]. In dilute solution, emission was assigned either to a ^{3}LC or a ^{3}MLCT state[3,4,9], but in more concentrated solution aggregation gave rise to different emission maxima[14]. The Pt(II)bpy dicarbonyl complex was also found to undergo π-π stacking in the solid state resulting in electronic interactions associated with Pt···Pt orbital overlap[15]. The Pt(bph)(bpy) complex was reported in the past and the absorption spectrum showed a broad peak located at 429 nm (ε = 5700 $M^{-1}cm^{-1}$) plus additional bands related to intraligand transitions at higher energy[3]. An emission maximum was observed at 581 nm with an emission lifetime of 1.1 µs at 77 K in a

butyronitrile glass upon excitation at 355 nm. The low energy absorption band was also reported to be solvent dependent[16].

Because these complexes absorb visible and UV light strongly, they may be of use in solar energy conversion**.** A donor/acceptor system is attempted to be made where the donor absorbs light, becomes excited, and transfers this energy to an acceptor as it relaxes back down to the ground state. Before such systems are to be prepared, the molecules themselves must be synthesized and characterized by their electrochemical behavior and UV/Visible spectra to determine if they may be useful.

The electronic process of a molecule absorbing and then emitting light can be explained by the use of a Jablonski Diagram, as shown in figure 1.1. This can be attributed to a metal to ligand charge transfer, which in the platinum series the ligand that receives the charge is the bipyridine or substituted bipyridine. When a sample is irradiated with light in the visible range, some of the light will have an energy equal to the first transition, the singlet ground state (S_o) to singlet excited state (S_1). This is due to an electron from the platinum moving to the bipyridine ligand. The electron will then eventually move back down to the ground state. In the case of the platinum series, the electron will first undergo intersystem crossing to the triplet state (T_o), and then back down to the ground state (S_o), in the process emitting energy as light.

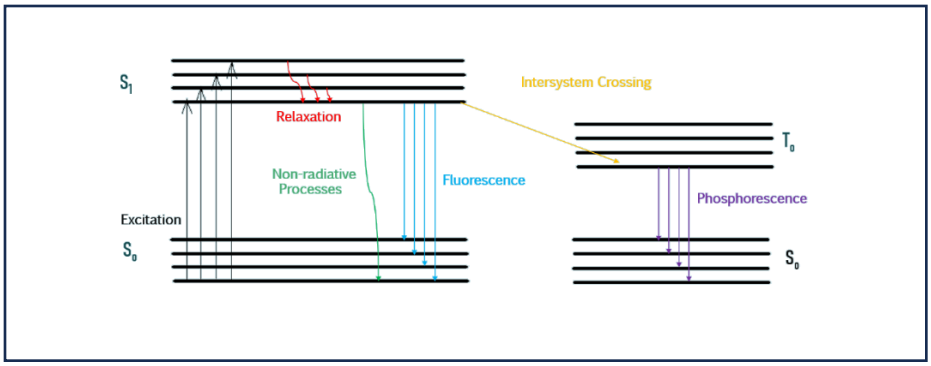

Figure 1.2 Jablonski Diagram

This thesis describes our goal of obtaining a better understanding of the electronic structures and photophysical properties of Pt(bph)(bpy). A modified synthetic procedure for the synthesis of Pt(bph)(bpy) is given, and their single crystal X-ray structures, spectroscopic and luminescence properties are described. The strong field dianionic bph ligand is expected to drive up the energy of the d-d state on the metal center enhancing emission and to have higher π* energy levels than those of diamine ligands. Consequently, the LUMO is expected to reside on the bpy ligands, which can and have been verified by DFT and TDDFT calculations[7].

CHAPTER 2

SYNTHESIS OF COMPOUNDS

2.1 Starting Materials and Instrumentation

Materials: All syntheses were performed under a dry and oxygen-free nitrogen atmosphere using standard Schlenk-tube techniques. Methylene chloride and hexanes were purchased from Fisher Scientific and were used as received. Anhydrous diethyl ether (99.7%) was used as received from Aldrich. The bipyridine substituted ligands were commercially purchased and used as received.

Instrumentation and Physical Measurements: IR spectra were acquired using a Nicolet Avatar 360 FT-IR spectrophotometer. Proton NMR spectra were obtained using a Varian Inova 400 FT-NMR spectrometer. Elemental (C, H, & N) analysis was performed by Columbia Analytical Services, Tucson, AZ. An EG&G PAR Model 263A potentiostat/galvanostat was used to obtain the cyclic and differential-pulse voltammograms. The measurements were carried out in a typical H-cell using a platinum disk working electrode, a platinum wire counter electrode, and a $Ag/AgNO_3$ reference electrode in dichloromethane. The supporting electrolyte used was 0.1 M tetrabutylammonium hexafluorophosphate ($TBAPF_6$). Ferrocene was added as the reference. Absorption profile and extinction studies were carried out using an OLIS Cary 14 UV/Visible/NIR double beam spectrophotometer. All solution samples were prepared using spectral grade acetonitrile or freshly distilled butyronitrile.

Emission spectra, excitation spectra and emission lifetimes were obtained using a FL3-2iHR Nanolog spectrometer from Horiba Jobin Yvon Technologies. Solutions with an absorbance

of ~0.1 at the λ_{max} of each complex in butyronitrile were placed in Pyrex tubes (5mm OD; 3 mm ID) and freeze-pump-thaw degassed. After the final degassing, the glassy samples were placed in a Dewar located in the cavity of the spectrometer and maintained at 77 K during measurements. Emission spectra were collected at λ_{max} of the MLCT bands; excitation spectra were obtained at the emission maximum for each compound. A NanoLED-460 pulsed diode light source was used in all lifetime decay determinations. In this case the excitation wavelength used was set to 457 nm – the absorption maximum for the NanoLED-460 light source. Emission curve-fittings were performed using the Origin Pro 8 program™ via non-linear curve-fitting modes.

2.2 Synthesis of main precursor – $[Pt(bph)(Et_2S)]_2$

The preparation of the biphenyl dianion is shown in Figure 2.1 followed by the procedure.

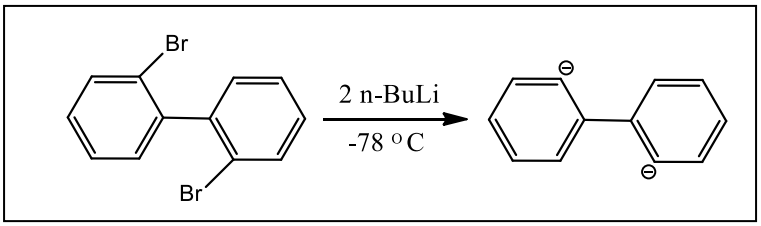

Figure 2.1: Removal of bromines from dibromobenzene to form a dianion

840 mg (2.6 mmol) of 2, 2'-dibromobiphenyl was placed into a 200 mL round-bottom flask along with a stirring bar. A serum cap was placed on the flask and then connected to a dropping funnel by use of a T-tube connector. The apparatus was evacuated and refilled with N_2 several times. Dry ether (approx. ~ 40 mL) was cannulated into the flask which was then

placed into a dry ice/isopropanol bath to lower the temperature to around -78° C. 2.1 mL of a 2.5 molar n-BuLi in hexane solution (5.2 mmol) was added by syringe dropwise over a two-hour period. The solution was then allowed to warm to 0° and stand before being transferred to the dropping funnel for use in the synthesis of platinum complexes.

The synthetic scheme for preparation of cis- $PtCl_2(SEt_2)_2$[13] is shown in Figure 2.2.

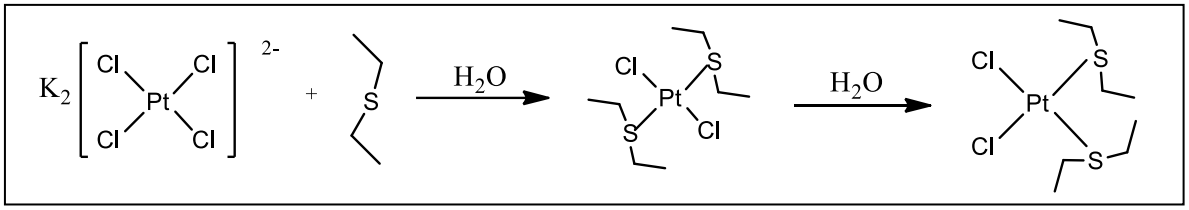

Figure 2.2: Synthesis of $PtCl_2(SEt_2)_2$

4.15 grams (.01 moles) of K_2PtCl_4 was placed in a 250 mL Erlenmeyer flask along with 50 mL water. 4.31 mL (.04 moles) of diethyl sulfide was added slowly to the flask. A serum cap was placed on the flask and was shaken until the original dark red solution had become colorless (approx. 10-15 minutes). The solution was then allowed to stir at room temperature for 24 hours. The resulting yellow solution was filtered and placed in an evaporating dish until it came to dryness. The resulting yellow solid was dissolved in 50-60 mL of hot benzene and then filtered to remove potassium chloride. The volume of the benzene solution was then reduced by about half and then placed in an ice bath until yellow crystals formed which were then separated by suction filtration.

The synthetic scheme of $[Pt(SEt_2)(bph)]_2$ is shown in Figure 2.3 and the preparation procedure follows it.

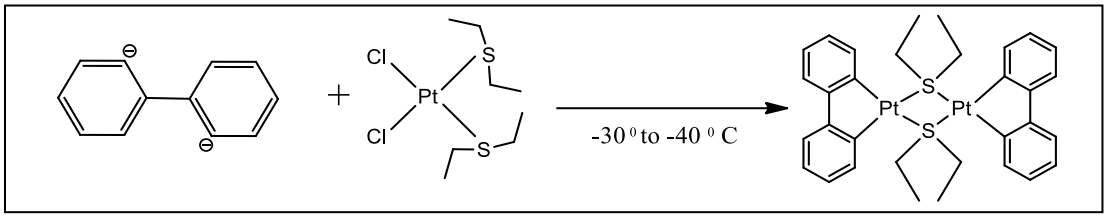

Figure 2.3: Synthesis of $[Pt\ (SEt_2)\ (bph)]_2$

A flask was prepared containing 1.2 grams cis- $PtCl_2(SEt_2)_2$ and 40 mL dry ether. A serum cap was placed on the flask. It was evacuated and refilled with N_2 several times. The serum cap was then removed from the flask and rapidly connected to a dropping funnel. The entire system was then evacuated and flushed with N_2 several times. The flask containing the cis-$PtCl_2(SEt_2)_2$/ether was then placed in a dry ice/ethylene glycol bath to lower the temperature to minus 30-40 °C. The contents of the dropping funnel were then added to the flask over a two-hour period. Stirring was continued for another hour and then the solution was allowed to slowly come to room temperature, after which it was is then filtered. A brownish solid is obtained on the filter which was purified by extraction with benzene.

2.3 Synthesis of platinum compounds with various ligands having substituents in the 4,4' positions of the 2,2,-bipyridine ligand

The synthetic schemes of a series of Pt(bph)(4,4'-X_2-2,2'bpy) complexes are shown in Figure 2.4 and synthetic procedures are outlined below it.

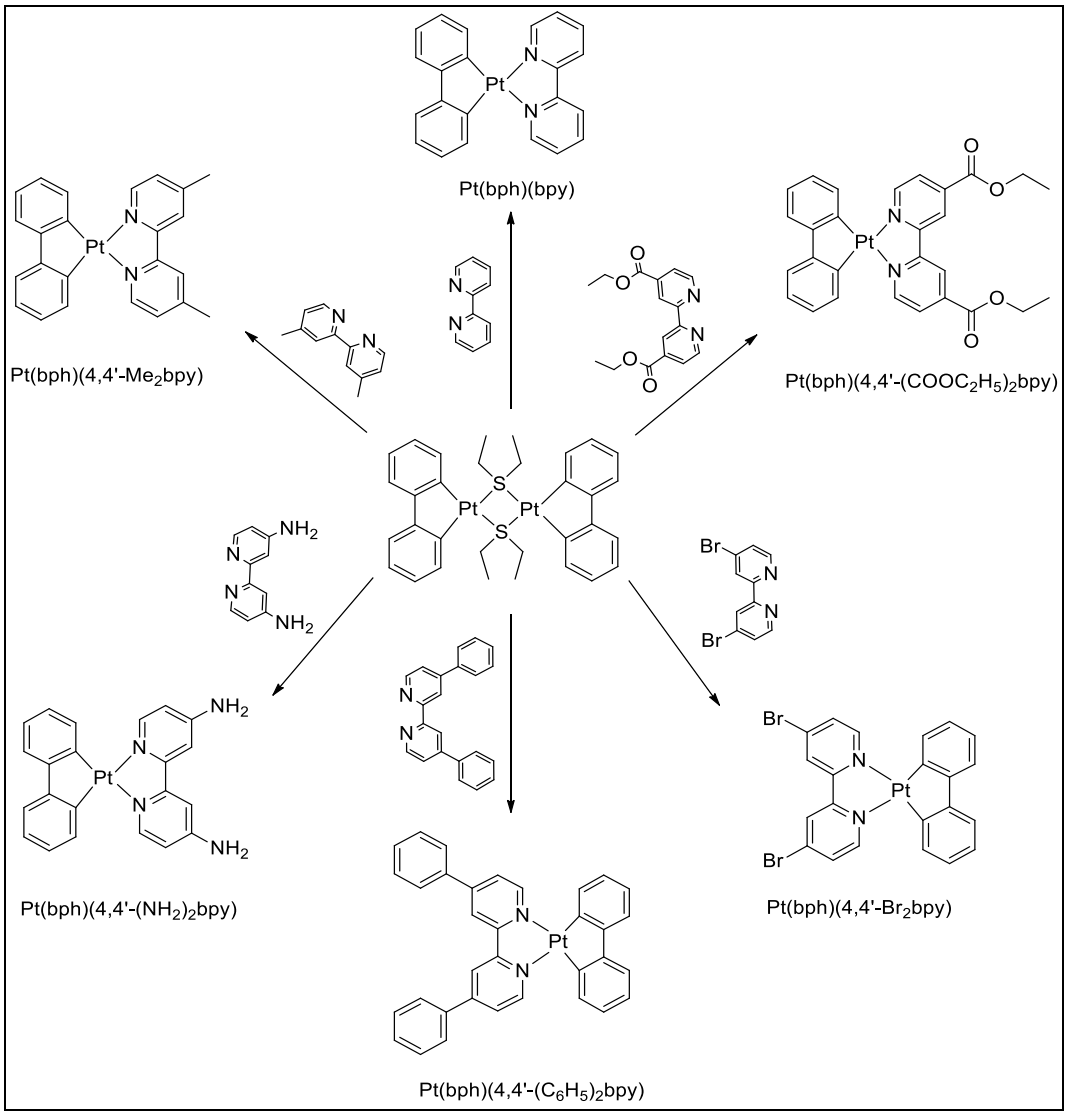

Figure 2.4: Schematic of forming derivatives of Pt(bph)(4,4'-X_2bpy)
(X = H, CH_3, Br_2, NH_2, Ph, EtCOO)

Pt(bph)(4,4'-Me_2bpy): A solution of 4,4'-dimethylbipyridine (46 mg, 0.25 mmol) in methylene chloride (10 mL) was added dropwise to a solution of $[Pt(bph)(C_2H_5)_2S]_2$ (100 mg, 0.114 mmol) in methylene chloride (20 mL) under continuous stirring. The brown colored reaction mixture was allowed to stir at room temperature for half an hour, rotary-evaporated to about 10 mL and added dropwise to 500 mL hexanes. The brown colored precipitate was isolated, vacuum filtered and washed with ether. Yield: 66 mg (50%) Anal. Calcd for $C_{24}H_{20}N_2Pt$: C, 54.23; H, 3.79; N, 5.27. Found for $C_{24}H_{20}N_2Pt$: C, 53.94; H, 4.20; N, 5.25. IR (KBr pellet): 3040, 1616, 1417, 1034, 830, 739, 521 cm^{-1}. ^1H NMR ($CDCl_3$): δ ppm 9.39 (d, 2H, J = 5.6 Hz), 7.84 (s, 2H), 7.43 (d, 2H, J = 5.6 Hz), 7.42 (dd, 2H, J = 6.8, 2.0 Hz), 7.38 (dd, 2H, J = 6.8, 2.0 Hz), 7.00 (td, 2H, J = 6.8, 2.0 Hz), 6.94 (td, 2H, J = 6.8, 2.0 Hz), 2.41 (s, 6H).

Pt(bph)(4,4'-Ph_2bpy)·$3H_2O$: Both 4,4'-diphenylbipyridine (18 mg, 0.06 mmol) and $[Pt(bph)(C_2H_5)_2S]_2$ (25 mg, 0.03 mmol) were added to a round-bottomed flask with a stir bar. Then 5 mL of dichloromethane was added and the mixture was allowed to stir at 40 C for 3 h. The solution was then filtered to remove solid impurities and the filtrate was evaporated to dryness. The solid was redissolved in a small amount of methylene chloride and added to ether to precipitate the compound. The precipitate was removed by vacuum filtration, washed with ether and dried under vacuum. It was then dissolved in methylene chloride and passed over a silica gel column for purification. Yield: 20 mg (51%) Anal. Calcd for $C_{34}H_{32}N_2O_3Pt$: C, 57.38; H, 4.53; N, 3.94. Found for $C_{34}H_{32}N_2O_3Pt$: C, 57.49; H, 3.71; N, 3.96. IR (KBr pellet): 3043, 1610, 1580, 1466, 1412, 1054, 761, 740, 731, 693 cm^{-1}. ^1H NMR ($CDCl_3$): δ ppm 9.58 (d, 2H, J = 5.6 Hz), 8.29 (d, 2H, J = 1.6 Hz), 7.75 (m, 10H), 7.55 (dd, 2H, J = 5.6, 1.6 Hz), 7.47 (dd, 2H, J = 6.8, 2.0 Hz),

7.34 (dd, 2H, J = 6.8, 2.0 Hz), 6.97 (m, 4H, J = 6.8, 2.0 Hz).

Pt(bph)(4,4'-$(NH_2)_2$bpy)·$2H_2O$: Both 4,4'-diaminobipyridine (11 mg, 0.06 mmol) and $[Pt(bph)(C_2H_5)_2S]_2$ (25 mg, 0.03 mmol) were added to a round-bottomed flask with a stir bar. Then 5 mL of dichloromethane was added, and the mixture allowed to stir at 40 C for 3 h. During this time a yellow precipitate formed. The solid was removed by vacuum filtration, washed with ether and dried under vacuum. Yellow needles were obtained by recrystallization in methanol. Yield: 17 mg (63%) Anal. Calcd for $C_{22}H_{22}N_4O_2Pt$: C, 46.40; H, 3.89; N, 9.84. Found for $C_{22}H_{22}N_4O_2Pt$: C, 46.30; H, 3.97; N, 9.62. IR (KBr pellet): 3043, 1610, 1580, 1466, 1412, 1054, 761, 740, 731, 693 cm^{-1}. ^{1}H-NMR (DMSO): δ ppm 8.68 (d, 2H, J = 5.6 Hz), 7.30 (dd, 2H, J =5.6, 1.6 Hz), 7.24 (d, 2H, J =5.6), 7.16 (dd, 2H, J = 6.8, 2.0 Hz), 6.99 (d, 2H, J = 6.8), 6.81 (td, 2H, J = 6.8, 2.0 Hz), 6.75 (m, 2H, J = 6.8, 2.0 Hz).

Pt(bph)(4,4'-Br_2bpy)·$5H_2O$: Both 4,4'-dibromobipyridine (19 mg, 0.06 mmol) and $[Pt(bph)(C_2H_5)_2S]_2$ (25 mg, 0.03 mmol) were added to a round-bottomed flask with a stir bar. Then 5 mL of dichloromethane was added, and the mixture was allowed to stir at 40 C for 3 h. The orange color precipitate was isolated and washed with ether. Yield: 18 mg (48%) Anal. Calcd for $C_{22}H_{24}N_2O_5Br_2Pt$: C, 35.17; H, 3.22; N, 3.73. Found for $C_{22}H_{24}N_2O_5Br_2Pt$: C, 35.00; H, 2.87; N, 3.67. IR (KBr pellet): 3043, 1610, 1580, 1466, 1412, 1054, 761, 740, 731, 693 cm^{-1}. ^{1}H-NMR ($CDCl_3$): δ ppm 9.42 (d, 2H, J = 5.6 Hz), 8.16 (d, 2H, J = 5.6 Hz), 7.75 (dd, 2H, J = 5.6, 1.6), 7.31 (dd, 2H, J = 6.8, 2.0 Hz), 7.17 (dd, 2H, J = 6.8, 2.0 Hz), 6.98 (dd, 2H, J = 6.8, 2.0 Hz), 6.89 (dd, 2H, J = 6.8, 2.0 Hz).

Pt(bph)(4,4'-($COOC_2H_5$)$_2$bpy): A solution of 4,4'-diethylesterbipyridine (75 mg, 0.25 mmol) in methylene chloride (10 mL) was added drop-wise to a solution of [Pt(bph)(C_2H_5)$_2$S]$_2$ (100 mg, 0.114 mmol) in methylene chloride (20 mL) under continuous stirring. The reaction mixture was stirred at room temperature for half an hour and then rotary-evaporated to reduce its volume to about 10 mL. The purple crystals that formed were removed by vacuum filtration, washed with ether and dried under vacuum. Yield: 81mg (50%) Anal. Calcd for $C_{28}H_{28}N_2O_4Pt$: C, 51.61; H, 4.33; N, 4.30. Found for $C_{28}H_{28}N_2O_4Pt$: C, 52.12; H, 4.11; N, 4.36. IR (KBr pellet): 3038, 2984, 1731, 1365, 1326, 1252, 1022, 761, 734 cm^{-1}. ^{1}H-NMR (CD_2Cl_3): δ ppm 9.40 (d, 2H, J = 5.6 Hz), 8.20 (d, 2H, J = 1.6 Hz), 7.83 (dd, 2H, J = 5.6, 1.6 Hz), 7.09 (dd, 2H, J = 7.2, 2.0 Hz), 7.02 (dd, 2H, J = 7.2, 2.0 Hz), 6.78 (td, 2H, J = 7.2, 2.0 Hz), 6.58 (td, 2H, J = 7.2, 2.0 Hz), 4.49 (q, 4H, J = 7.2 Hz), 1.51 (t, 6H, J = 7.2 Hz).

CHAPTER 3

CRYSTAL STRUCTURES OF PLATINUM(II) BIPHENYL COMPLEXES

The single crystal X-ray diffraction studies were carried out on a Bruker Kappa APEX-II CCD diffractometer equipped with Mo K_α radiation (α= 0.71073 Å).[18] Crystals were mounted on a Cryoloop with Paratone-n oil. Data were collected in a nitrogen gas stream at 100 or 150 K using ϕ and ϖ scans. Crystal-to-detector distance was 45 or 50 mm and exposure time was 5 or 10 seconds per frame using a scan width of 0.5 or 1.0°. Data collection was ~100% complete to 25.00° in θ for each structure. The data were integrated using the Bruker SAINT Software program and scaled using the SADABS software program[18]. Solution by direct methods (SHELXS or SHELXT) produced a complete phasing model consistent with the proposed structure. Crystallographic determination data for the compounds are collected in Table 3.1.

All nonhydrogen atoms were refined anisotropically by full-matrix least-squares (SHELXL-2014). All hydrogen atoms were placed using a riding model. Their positions were constrained relative to their parent atom using the appropriate HFIX command in SHELXL-2014. The Pt(bph)(4,4'-Me_2bpy) complex sits on a general position in the monoclinic space group $P2_1/n$; Pt(bph)(4,4'-Br_2bpy) sits on a general position in an orthorhombic space group *Pbca* and Pt(bph)(4,4'-$(COOC_2H_5)_2$bpy) on a general position in the monoclinic space group $C2/c$.

3.1 Crystal data of $PtCl_2(Et_2S)_2$ and $[Pt(bph)(Et_2S)]_2$

Diagrams of $PtCl_2(Et_2S)_2$ and $[Pt(bph)(Et_2S)]_2$ along with their crystal structures are shown in Figure 3.1. Table 3.1 contains crystal data for the two complexes.

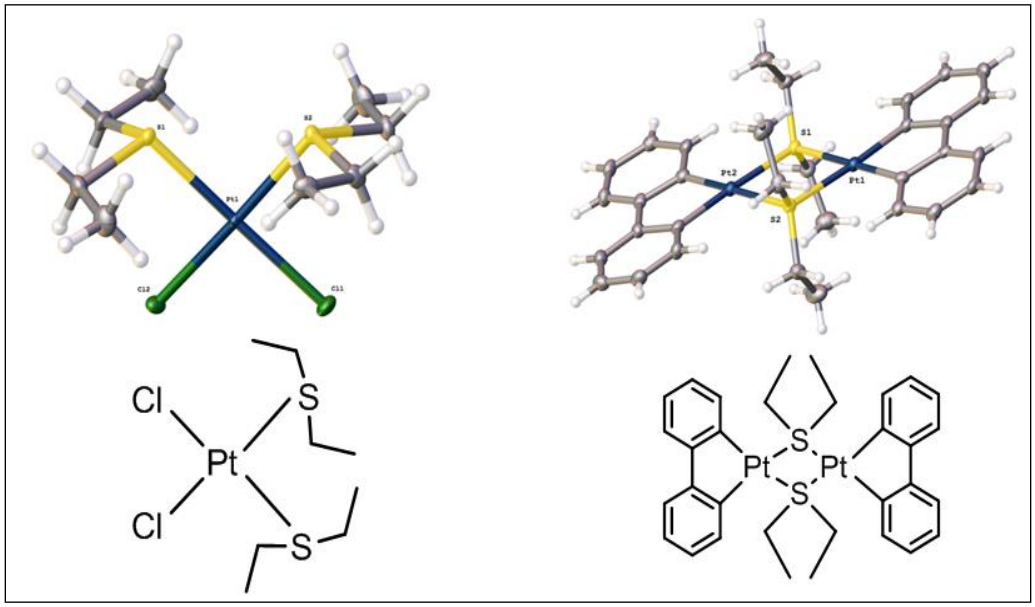

Figure 3.1 Diagrams of $PtCl_2(Et_2S)_2$ and $[Pt(bph)(Et_2S)]_2$ along with their crystal structures

Table 3.1 Crystal data of $PtCl_2(Et_2S)_2$ and $[Pt(bph)(Et_2S)]_2$

Molecular formula	C8 H20 Cl2 Pt S2	C32 H36 Pt2 S2
Formula weight	446.35	874.91
Temperature	100(2) K	100(2) K
Wavelength	0.71073 Å	0.71073 Å
Crystal system	Monoclinic	Monoclinic
Space group	P 21/n	P 1 21/n 1
Unit cell dimensions	a = 10.7068(4) Å	a = 19.2938(15) Å
	b = 11.1561(4) Å	b = 7.8839(6) Å
	c = 12.1730(5) Å	c = 19.6969(17) Å
	α = 90°.	α = 90°.
	β = 101.8520(10)°.	β = 109.639(5)°.
	γ = 90°.	γ = 90°.
Volume	1423.02(9) $Å_3$	2821.8(4) $Å_3$
Z	4	4
Density (calculated)	2.083 Mg/m_3	2.059 Mg/m_3
Absorption coefficient	10.492 mm_{-1}	10.072 mm_{-1}
F(000)	848	1664
Crystal size	0.080 x 0.050 x 0.020 mm_3	0.053 x 0.015 x 0.011 mm_3
Crystal color, habit	Colorless Plate	Yellow Rod
Theta range for data collection	2.310 to 28.283°.	2.807 to 28.333°.
Index ranges	-14<=h<=13, -14<=k<=14, -13<=l<=15	-23<=h<=25, -10<=k<=10, -26<=l<=26
Reflections collected	16900	39401
Independent reflections	3454 [R(int) = 0.0316]	6763 [R(int) = 0.0575]
Completeness to theta = 25.000°	99.90%	99.80%
Absorption correction		Semi-empirical from equivalents
Max. and min. transmission	0.7457 and 0.5063	0.0656 and 0.0278
Refinement method	Full-matrix least-squares on F_2	Full-matrix least-squares on F_2
Data / restraints / parameters	3454 / 0 / 122	6763 / 0 / 329
Goodness-of-fit on F_2	1.037	1.031
Final R indices [I>2sigma(I)]	R1 = 0.0183, wR2 = 0.0308	R1 = 0.0333, wR2 = 0.0710
R indices (all data)	R1 = 0.0247, wR2 = 0.0323	R1 = 0.0456, wR2 = 0.0752
Extinction coefficient	n/a	n/a
Largest diff. peak and hole	0.605 and -0.791 $e.Å_{-3}$	1.796 and -1.949 $e.Å_{-3}$

3.2 Crystal structure data of Pt(bph)(4,4'-Me_2bpy), Pt(bph)(4,4'-Br_2bpy) and Pt(bph)(4,4'-($COOC_2H_5$)$_2$bpy).

Crystal structures of Pt(bph)(4,4'-Me_2bpy), Pt(bph)(4,4'-Br_2bpy) and Pt(bph)(4,4'-($COOC_2H_5$)$_2$bpy) are shown in Figure 3.2 and Table 3.2 lists crystal structure data.

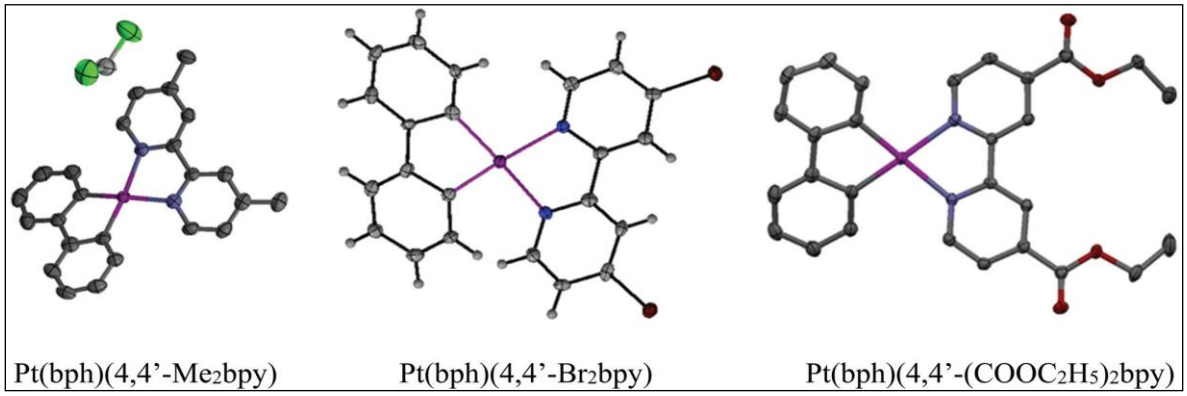

Figure 3.2 Crystal structures of Pt(bph)(4,4'-Me_2bpy), Pt(bph)(4,4'-Br_2bpy) and Pt(bph)(4,4'-($COOC_2H_5$)$_2$bpy)

Table 3.2 Crystal Structure Data of Pt(bph)(4,4'-Me_2bpy), Pt(bph)(4,4'-Br_2bpy) and Pt(bph)(4,4'-($COOC_2H_5$)$_2$bpy)

Identification code	Pt(bph)(4,4'-Me_2bpy)	Pt(bph)(4,4'-Br_2bpy)	Pt(bph)(4,4'-($COOC_2H_5$)$_2$bpy)
Empirical formula	$C_{23}H_{20}N_2Pt_1 \bullet CH_2Cl_2$	$C_{22}H_{14}Br_2N_2Pt$	$C_{28}H_{24}N_2O_4Pt_1$
Formula weight	616.44	661.26	647.58
Temperature	150 K	100 K	150 K
Wavelength	0.71073 Å	0.71073	0.71073 Å
Crystal system	Monoclinic	Orthorhombic	Monoclinic
Space group	$P2_1/n$	Pbca	C2/c
Unit cell dimensions	a = 13.7375(5) Å	a = 7.2532(7) Å	a = 22.3019(11) Å
	b = 9.7822(4) Å	b = 20.093(4) Å	b = 7.1519(4) Å
	c = 17.1526(7) Å	c = 24.757(6) Å	c = 31.0906(15) Å
	α = 90°	α = 90°	α = 90°

TABLE 3.2 (continued)

	$\beta = 111.300(2)°$	$\beta = 90°$	$\beta = 105.466(3)°$
	$\gamma = 90°$	$\gamma = 90°$	$\gamma = 90°$
Volume	2147.56(15) $Å^3$	3608.0(14) $Å^3$	4779.4(4) Å3
Z	4	8	8
Calculated density	1.907 g/cm^3	2.435 g/cm^3	1.800 g/cm3
Absorption coefficient	6.798 mm^{-1}	12.217 mm^{-1}	5.910 mm-1
F(000)	1192	2464	2528
Crystal size	0.33 x 0.23 x 0.04 mm	0.153 x 0.01 x 0.008 mm	0.33 x 0.25 x 0.18 mm
Crystal habit	Plate	Needle	Plate
Crystal color	Clear Light Red	Orange	Lustrous Dark Purple
θ range for data collection	1.64^o to 26.00^o	2.027^o to 26.428^o	3.40^o to 26.00^o
Limiting indices	$-16 \leq h \leq 16$ $-12 \leq k \leq 12$ $-21 \leq l \leq 21$	$-5 \leq h \leq 9$ $-17 \leq k \leq 25$ $-29 \leq l \leq 30$	$-27 \leq h \leq 27$ $-8 \leq k \leq 8$ $-38 \leq l \leq 38$
Reflections collected / unique	51173 / 4209 [R(int) = 0.0330]	18727/3689 [R(int) = 0.0726]	54008 / 4700 [R(int) = 0.0472]
Completeness to $\theta = 26.00$	100 %	99.9%	99.8 %
Refinement method	Full-matrix least-squares on F^2	Full-matrix least-squares on F^2	Full-matrix least-squares on F^2
Data / restraints / parameters	4209 / 0 / 273	3689/ 0 /244	4700 / 0 / 318
Refinement threshold	$I>2\sigma(I)]$	$I>2\sigma(I)]$	$I>2\sigma(I)]$
Data > threshold	3865	N/A	4351
Goodness-of-fit on F^2	1.404	1.036	1.163
Final R indices [$I>2\sigma(I)$]	R1 = 0.0157, wR2 = 0.0546	R1 = 0.0379, wR2 = 0.0644	R1 = 0.0235, wR2 = 0.0571
R indices (all data)	R1 = 0.0221, wR2 = 0.0923	R1 = 0.0580, wR2 = 0.0703	R1 = 0.0262, wR2 = 0.0584
Largest diff. peak and hole	0.966 and -1.180 $e^- Å^{-3}$	0.821 and -1.138 $e^- Å^{-3}$	1.379 and -2.170 $e^- Å^{-3}$

Selected bond distances and angles measured using XRD for single crystals are listed in Table 3.3. The complex with an unsubstituted bpy is also included for comparison. The results show that the Pt-N bonds are longer than the Pt-C bonds by ~0.10-0.12 Å. The C-Pt-C bite angles are ~80° and the N-Pt-N bite angles are 3° smaller at 77°. The torsion angle between the best-fit planes of the biphenyl and 4,4'-bipyridine moieties, referred to as bpy-bph, is particularly important for the evaluation of distortion of these pseudo square-planar complexes from planarity. The bpy-bph torsion angles in the crystal structures of Pt(bph)(Me_2bpy), Pt(bph)(4,4'-Br_2bpy) and Pt(bph)(4,4'-($COOC_2H_5$)$_2$bpy) are close to that of the previously reported Pt(bph)(bpy)[11] complex, highlighting the X-configuration characteristic to these distorted pseudo square-planar complexes of Pt(II).[19] It is important to note that Pt(bph)(4,4'-Br_2bpy) and Pt(bph)(4,4'-($COOC_2H_5$)$_2$bpy) as well as Pt(bph)(bpy)[15] form dimers stacked along the axis perpendicular to the approximate plane of the complex and passing through the Pt atom, whereas the dimers of Pt(bph)(Me_2bpy) are in parallel displaced configuration with only the Me_2bpy moieties stacked. In the dimers, the bpy ligands are stacked together in Pt(bph)(bpy),[15] whereas the ($COOC_2H_5$)$_2$bpy ligands are stacked oppositely in Pt(bph)(4,4'-($COOC_2H_5$)$_2$bpy). The latter stacking mode is similar to that of the Pt(bph)(CO)$_2$ complex reported previously.[13,14]

Table 3.3 Selected Bond Lengths (Å), Bond Angles (°) and Torsion Angles (°) Measured Using XRD crystallography.

Measured	Pt(bph)(4,4'-Me_2bpy)	Pt(bph)(bpy)	Pt(bph)(4,4'-Br_2bpy)	Pt(bph)(4,4'-$(COOC_2H_5)_2$bpy)
		Bond length		
Pt – C1	2.006(8)	1.993 (9)	1.994(7)	2.009(4)
Pt – C2	2.016(9)	2.021(10)	2.006(7)	2.002(4)
Pt – N1	2.125(6)	2.101(8)	2.112(5)	2.118(3)
Pt – N2	2.113(6)	2.125(8)	2.128(4)	2.129(3)
		Bond angle		
C1 – Pt – C2	80.6(3)	80.2(4)	81.0(3)	80.5(3)
N1 – Pt – N2	77.3(2)	76.6(3)	77.5(2)	77.4(1)
C1 – Pt – N1	102.3(3)	102.5(3)	102.3(2)	102.3(1)
C2 – Pt – N2	102.8(3)	104.1(3)	103.0(2)	102.7(1)

The side view for crystal structures of Pt(bph)(4,4'-Me_2bpy), Pt(bph)(4,4'-H_2bpy) Pt(bph)(4,4'-Br_2bpy) and Pt(bph)(4,4'-($COOC_2H_5$)$_2$bpy) are shown in Figure 3.3. The bph and bpy rings are not collinear as anticipated but take up an X configuration. Apparently, the dπ orbitals are unable to facilitate binding both ligands in a linear fashion. This is likely due to steric interactions and repulsion of substituted ligands. As can be seen in the figure, as the substituted ligands get larger or bulkier, there is more of a deviation from planarity.

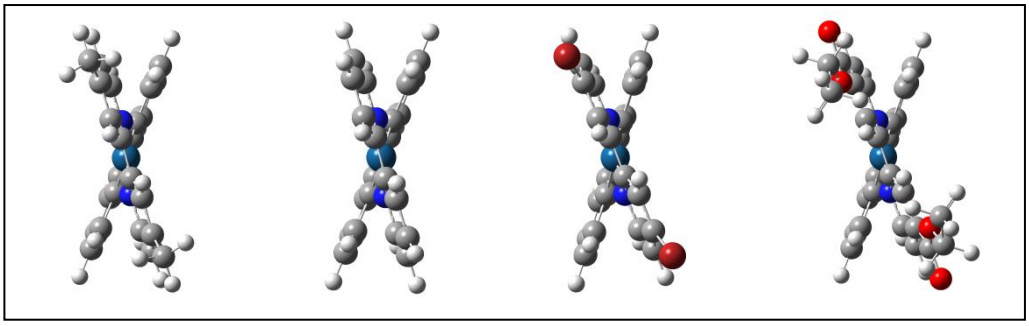

Figure 3.3 Crystal structures of Pt(bph)(4,4'-Me_2bpy), Pt(bph)(4,4'-H_2bpy) Pt(bph)(4,4'-Br_2bpy) and Pt(bph)(4,4'-($COOC_2H_5$)$_2$bpy) showing their X configuration in the solid state

CHAPTER 4

ELECTRONIC PROPERTIES OF COMPOUNDS

4.1 Beer's Law Studies

Beer's law is given in equation 4.1, where A is the absorbance, Ɛ is the molar absorption coefficient, *l* is the path length (1cm), and c is the concentration. and was used to determine the molar absorption coefficients for the compounds.

$$A = Ɛlc \qquad (4.1)$$

The concentrations c of a given complex was varied, A was determined experimentally, and a plot of A *vs* c was constructed to determine Ɛ from the slope of the line.

An example of absorbance changes as function of concentration for Pt(bph)(4,4'-CH_3-bpy) is given in Figure 4.1 and a Beer's law plot at a fixed wavelength of A *vs* c is shown in Figure 4.2.

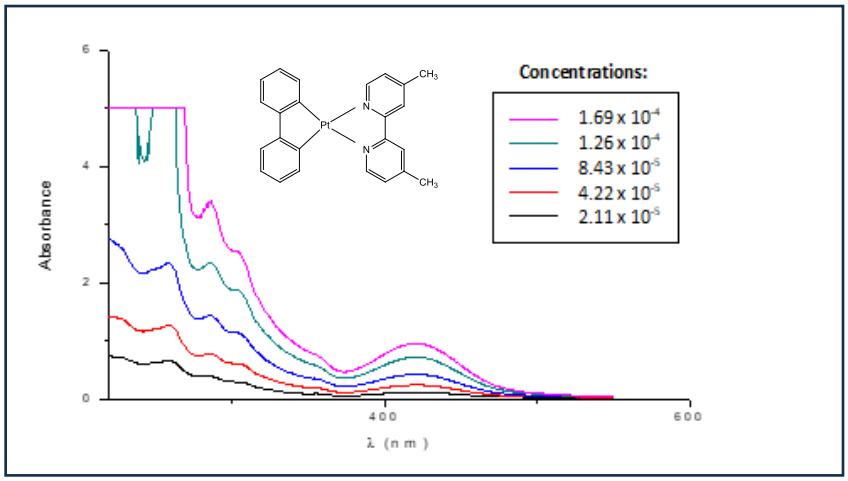

Figure 4.1 Absorbance changes vs concentration for Pt(bph)(4,4'-CH_3-bpy)

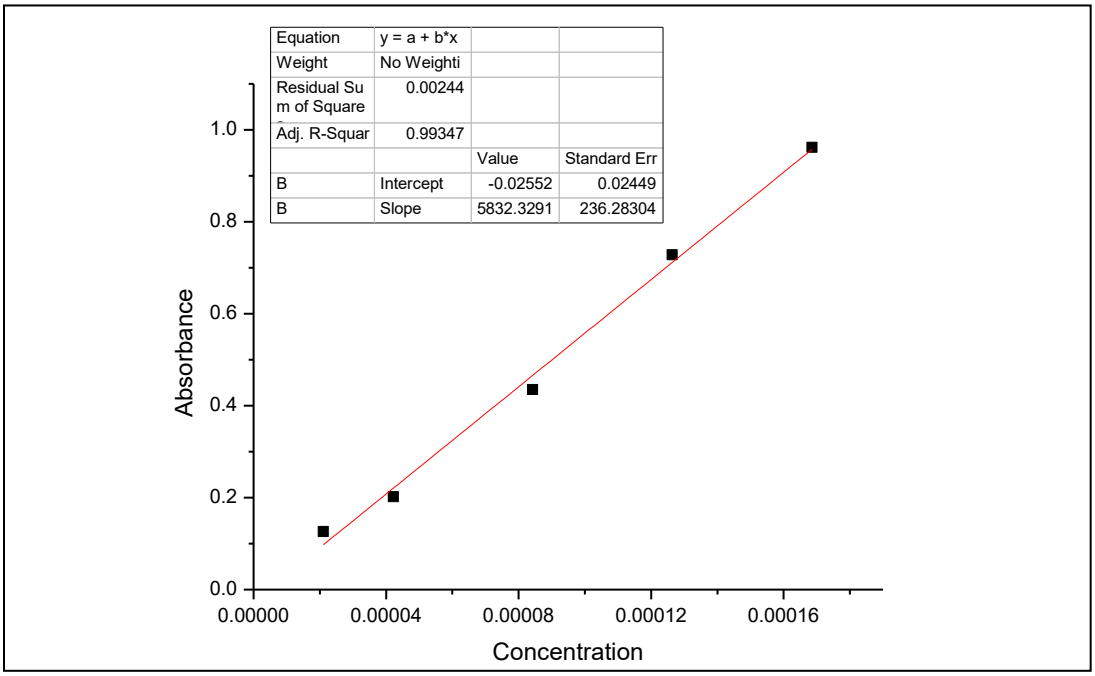

Figure 4.2 Beer's law plot of absorbance vs. concentration for Pt(bph)(4,4'-Me_2-bpy) in AN.

A linear relationship was obtained for the dimethyl substituted complex shown in Figure 4.2 with an R^2 value of .99347. The slope, 5832, is therefore equal to Ɛ.

4.2 UV/Visible Absorption Spectra

The lowest-energy bands of the absorption spectra of Pt(bph)(4,4'-X_2bpy) complexes are presented in Figure 4.3. These bands undergo bathochromic and hypsochromic shifts relative to the parent Pt(bph)(bpy) complex in the presence of electron-withdrawing and electron-donating substituents and fall in the energy series with X = NH_2 > CH_3 > H >Ph > Br > $COOC_2H_5$ consistent with the tabulated in Table 4.1. The absorption coefficients are in an intermediate range consistent with the characteristic metal-to-ligand charge transfer (MLCT) transitions.

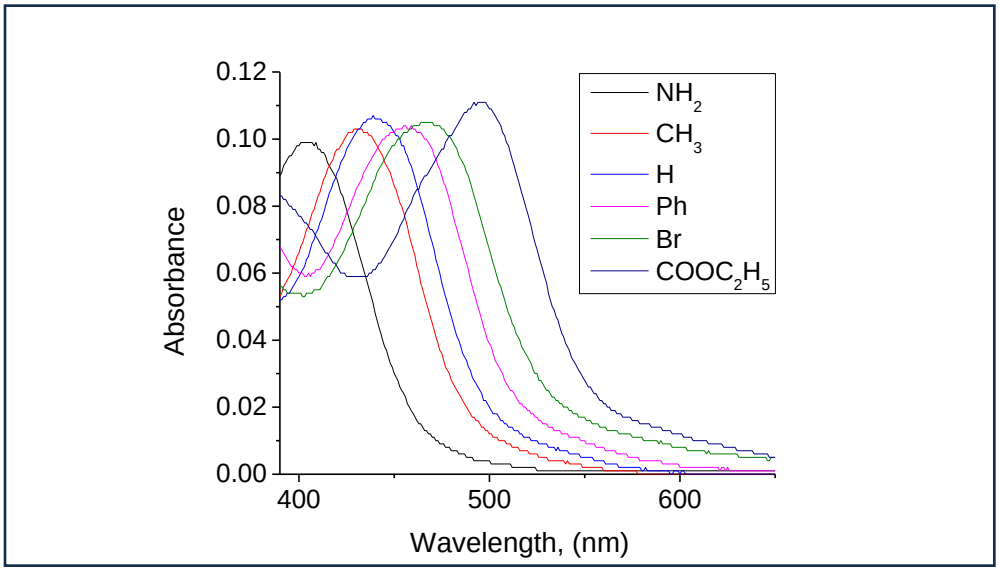

Figure 4.3 Experimental Absorption of Pt(bph)(4,4'-X_2bpy). Absorption spectra were obtained in butyronitrile at room temperature.

Table 4.1 Compounds and their absorption maxima and molar extinction coefficients

Compound	**λmax, nm**	**ε (L g^{-1} cm^{-1})**
Pt(bph)(4,4'-$(NH_2)_2$bpy)	405	3.6 x 10^3
Pt(bph)(4,4'-Me_2bpy)	420	6.1 x 10^3
Pt(bph)(bpy)	440	5.6x 10^3
Pt(bph)(4,4'-Br_2bpy)	470	6 x 10^3
Pt(bph)(4,4'-$(COOC_2H_5)_2$bpy)	500	8.2 x 10^3

4.3 Emission

Normalized emission spectra, presented in Figure 4.4, are broad with discernible vibronic coupling of approximately ~1156 – 1173 cm^{-1} as reported earlier for Pt(bph)(bpy)[5]. The emission energies of the complexes correlate well with the series found for absorption of the complexes. Excitation spectra were also collected and corresponded to the absorption profiles.

Experimental emission peak maxima and emission lifetimes for the complexes in a butyronitrile glass at 77 K are presented in Table 4.2. Emission is assigned to a triplet ^{3}MLCT to a ^{1}MLCT transition with partial π character. The largest emission lifetime of 2.25 μs was measured for Pt(bph)(4,4'-$(NH_2)_2$bpy) that features a distinctly more structured emission spectrum compared to the rest of the series. Long emission lifetimes are desirable for energy transfer applications.

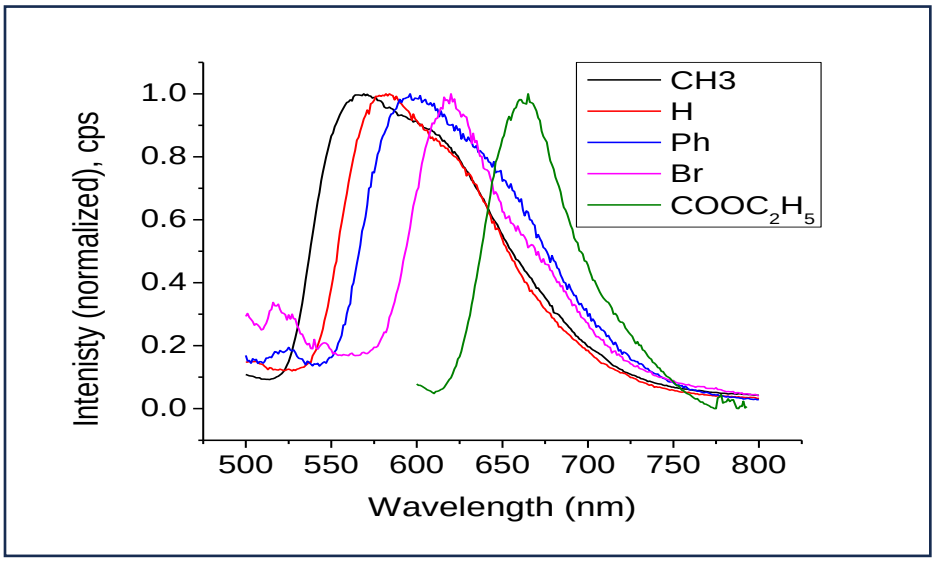

Figure 4.4 Experimental emission spectra of Pt(bph)(4,4'-X_2bpy), obtained in butyronitrile at 77 K.

Table 4.2 Experimental Emission Results

Complex	$\lambda_{abs,\ nm}^{a,b}$	$\lambda_{em,\ nm}^{c,d}$	$\tau,\ \mu s^{c,d}$
Pt(bph)(4,4'-$(NH_2)_2$bpy)	405	503	2.25
Pt(bph)(4,4'-Me_2bpy)	420	566	0.83
Pt(bph)(bpy)	456	584	0.69
Pt(bph)(4,4'-Br_2bpy)	470	620	0.37
Pt(bph)(4,4'-$(COOC_2H_5)_2$bpy)	500	670	0.17

a: in acetonitrile, b: room temperature, c: in butyronitrile, d 77K

4.4 Electrochemistry

Table 4.3 lists the half-wave reduction potentials E½ red determined for the complexes over the range of 0.0 V to -2.0 V vs. the $AgNO_3$ reference electrode. Within this range, Δ EP ,where Δ EP is the difference between the reduction and oxidation peak of the redox active couple determined by cyclic voltammetry, varied from 75 to 100 mV consistent with other reports found for one electron transfer processes in non-aqueous solvents. Irreversible electrochemical behavior was found in the range of 0 V to +2.0 V vs. the $AgNO_3$ reference electrode for the compounds and was not examined further. The solubility of Pt(bph)(4,4'-$(NH_2)_2$bpy) in dichloromethane was too low to study its electrochemical behavior. Figure 4.5 presents the differential pulse voltammograms of the complexes. The $E_{1/2}$ red values and voltammograms

shift to lower and higher voltages relative to Pt(bph)(bpy) in the presence of electron-withdrawing and electron-donating substituents, respectively, following the trends of the absorption and emission.

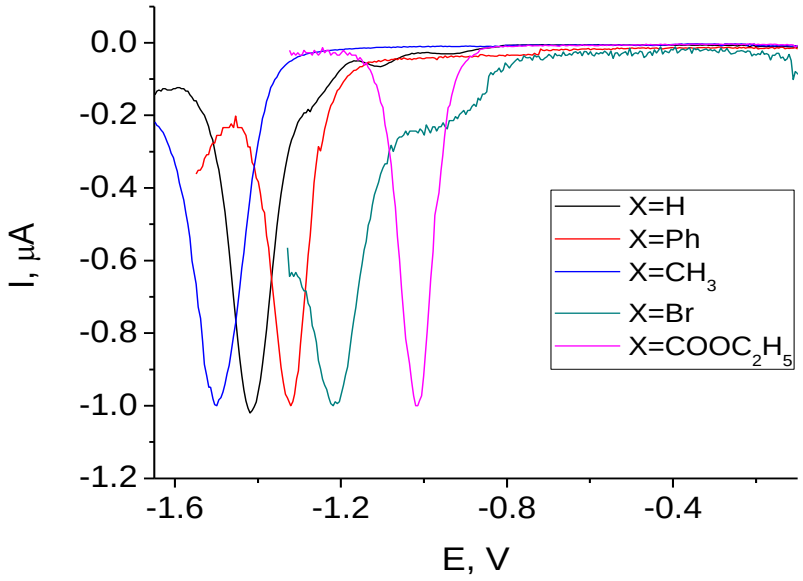

Figure 4.5 Differential pulse voltammograms of Pt(bph)(4,4'-X_2bpy) in butyronitrile.

Table 4.3 Electrochemical Reduction Potentials ($E_{1/2}$) of Pt(bph)(4,4'-X_2bpy) Complexes.

Complex	$E_{1/2red}$(V)[a]
Pt(bph)(4,4'-$(NH_2)_2$bpy)	NA[b]
Pt(bph)(4,4'-Me_2bpy)	-1.500
Pt(bph)(bpy)	-1.410
Pt(bph)(4,4'-Ph_2bpy)	-1.316
Pt(bph)(4,4'-Br_2bpy)	-1.209
Pt(bph)(4,4'-$(COOC_2H_5)_2$bpy)	-1.010

a: 0.1 M TBAH in dichloromethane b: Not available due to low solubility in dichloromethane

CHAPTER 5

FREE ENERGY CORRELATIONS

In order to further assess the effects of substituents on properties of the complexes in the series, linear correlations between experimental and computational results are examined with respect to Hammett sigma constants, σ, and in some cases with respect to each other. For consistency, only di-substituents that are para- with respect to the bipyridyl N atoms have been investigated (σ_p).

5.1 Absorption and Emission

The correlations of experimental lowest-energy transition and calculated ^{1}MLLCT SES (singlet excited states) for the complexes with σ_p presented in Figure 5.1 highlight the impressive agreement between theory and experiment. The energy of lowest-lying electronic transitions determined from both experiment and calculation increases in the order Pt(bph)(4,4'-$(COOC_2H_5)_2$bpy) < Pt(bph)(4,4'-Br_2bpy) < Pt(bph)(4,4'-Ph_2bpy) < Pt(bph)(bpy) < Pt(bph)(4,4'-Me_2bpy) < Pt(bph)(4,4'-$(NH_2)_2$bpy).

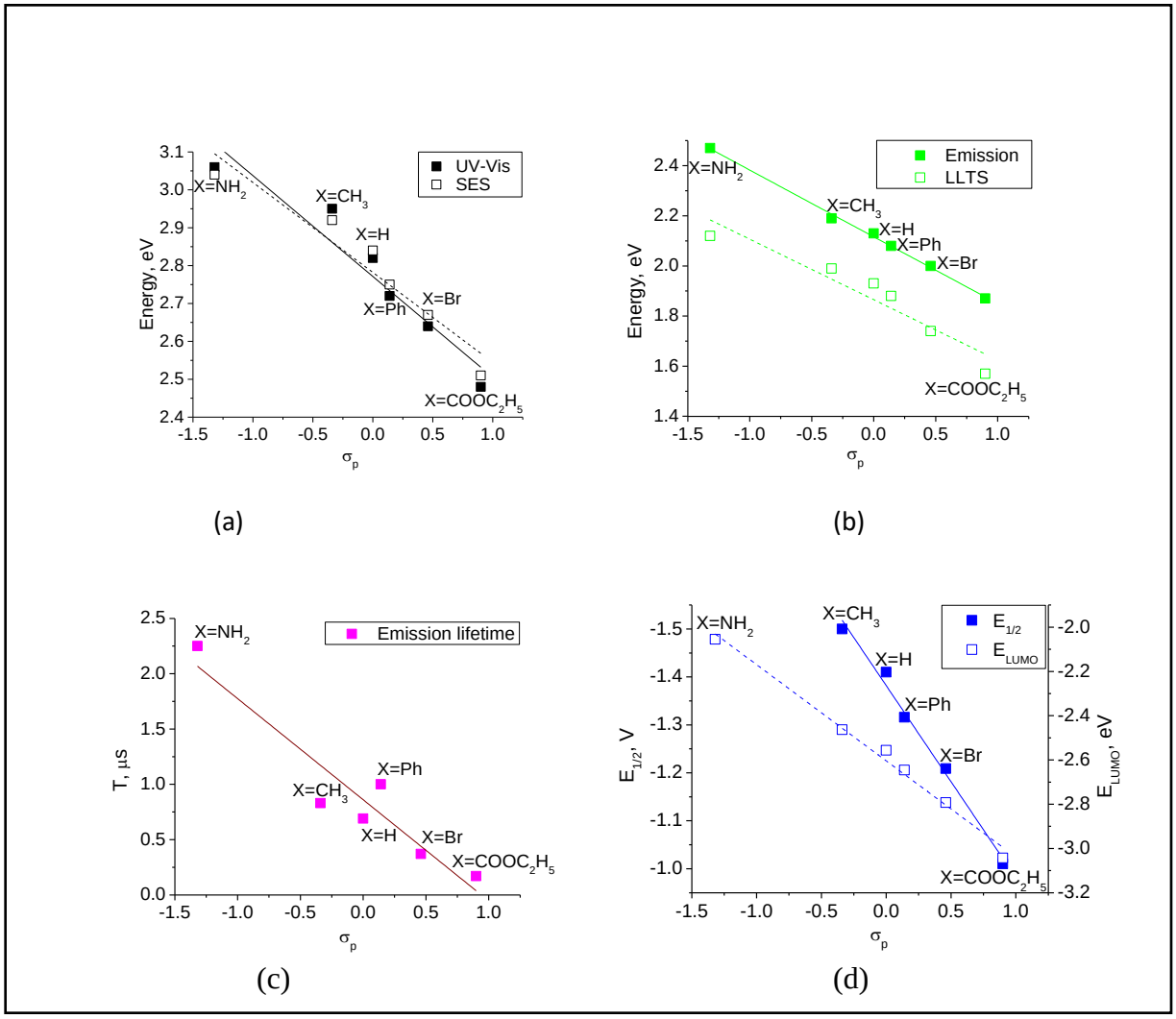

Figure 5.1 Experimental UV-Vis Absorption and Calculated ^{1}MLLCT State Energies *vs* σ_p (a), Experimental Emission and Calculated LLTS Energies *vs* σ_p (b), Experimental Emission Lifetime *vs* σ_p (c), and Electrochemical Reduction Potential $E_{1/2red}$ and E_{LUMO} *vs* σ_p (d) for the Pt(bph)(4,4'-X_2bpy) Complexes

The correlations of the experimental emission and calculated LLTS energies with σ_p are presented in Figure 5.1. These results show that the LLTS energies are systematically lower than the emission energies by 0.2 eV, which falls within the underestimation of 0.25 eV reported in the literature.[20,21] The linear fitting analysis results for absorption and emission (Figures 5.1(a) and 5.1(b) yield slopes in the relatively narrow range from -0.22 to -0.27. The intercepts for experimental emission and LLTS are lower than those for absorption by 0.7 eV and 0.9 eV,

respectively, representing estimates of the sum of the non-radiative relaxation energies for internal conversion and intersystem crossing. The emission lifetimes also correlate linearly with the Hammett constant, as shown in Figure 5.1(c), in agreement with an earlier report for para-substituted tetraphenyl porphyrin carbonyl complexes of ruthenium(II).[22] The emission spectrum of Pt(bph)(4,4'-$(NH_2)_2$bpy) features a shoulder at 584 nm (2.12 eV) and peaks at about 541 nm (2.29 eV) and 503 nm (2.47 eV). The spacing between the peaks is ~1400 cm^{-1} in the range previously attributed to ring breathing modes in transition metal complexes containing bipyridine ligands.[23]

5.2 Electrochemistry

Linear correlations of the electrochemical reduction potentials $E_{1/2red}$ with σ_p as shown in Figure 5.1(d) yield an impressive R^2 value of 0.99. Calculated absolute LUMO energies for complexes in acetonitrile solvent are also plotted *vs* σ_p in Figure 5.1(d) and give an R^2 value of 0.90. Electron-withdrawing substituents make the reduction of the complexes more thermodynamically favorable (have less negative $E_{1/2red}$) and correlate with lower E_{LUMO}. The opposite dependence holds for the electron-donating methyl substituent. Electron affinity, a more physical descriptor of a reduction potential that unlike the LUMO energy accounts for orbital relaxation, was also examined. The electron affinity, calculated as the total energy of the anion minus the total energy of the neutral complex, was found to correlate linearly with the Hammett σ_p.

5.3 Energy Gap Control

The HOMO-LUMO energy gap is a very important electronic structure characteristic of these complexes, as it is related to their photochemical and redox properties. The correlation of the HOMO-LUMO gap calculated using DFT with σ_p presented in Figure 5.2 indicates that by using electron-withdrawing and electron-donating substituents the properties of Pt(II) diimine complexes can be controlled to a large extent by using functional groups, as demonstrated by the R^2 value of 0.92.

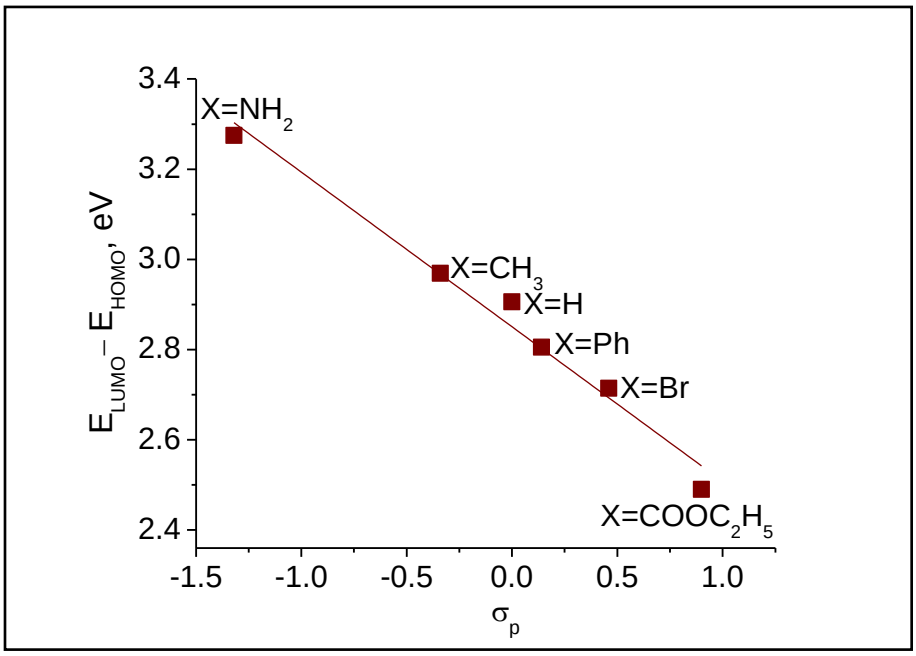

Figure 5.2 Calculated $E_{LUMO} - E_{HOMO}$ energy gap *vs* σ_p for Pt(bph)(4,4'-X_2bpy)

The HOMO-LUMO energy gap calculated using DFT gives a reasonable approximation of the lowest excitation energy without considering orbital relaxation[24]. The main source of error in energy gap calculations using DFT is the inaccuracy in the calculation of the LUMO energy. The

TD-DFT calculations yield vertical electronic energies of the SES and allow direct calculation of the HOMO-LUMO gap as the energy of the lowest-lying SES. However, lowest-lying excited states could be forbidden and not observed experimentally. The oscillator strength of an excited state computed using TD-DFT is related with molar absorptivity coefficient and allows identification of the lowest-energy transitions observable experimentally, e.g., using absorption UV-Visible spectroscopy.

CHAPTER 6

SUMMARY AND CONCLUSION

In conclusion, derivatives of Pt(bph)(bpy) with varying electron-withdrawing and donor substituents attached to the 4,4' positions of bipyridine have been synthesized and characterized. As noted from the results in Table 3.3, bond distances and bond angles from XRD in solid state show little dependence on substituent electron-donating and electron-withdrawal effects. However, these substituent effects are evident in the ^{1}H NMR spectra of the complexes. For Pt(bph)(4,4'-$(NH_2)_2$bpy), the bipyridyl ^{1}H chemical shifts appear mostly upfield at 7.24-8.68 ppm, while those of Pt(bph)(4,4'-$(COOC_2H_5)_2$bpy) are found downfield at 7.83-9.40 ppm.

The XRD results and geometry optimization using DFT showed that all the complexes in the series have an X-configuration with torsion angles of 28-30° in single crystals. Molecular orbital diagrams show that the HOMOs have Pt-biphenyl character and the LUMOs are localized on the bipyridyl group. Electron-donating and withdrawing effects were analyzed using Pt atom charge and spin density analyses. The lowest-lying triplet states were also optimized and assigned based on the localization of the electron spin density. The TD-DFT method was employed to predict the singlet excited states in acetonitrile that were found to be in very good agreement with the electronic absorption spectral peaks in the same solvent.

Correlations of calculated and experimental results with the Hammett constants for para-substitution position were established to analyze the electron-withdrawing and donating effects on the coordination sphere of the complexes in the series. The correlations of calculated ^{1}MLLCT

and UV-Visiblee spectra lowest-energy bands with the Hammett σ_p constants highlighted these charge transfer effects. The calculated LUMO energies as well as measured reduction half-wave potentials and emission lifetimes were also correlated with σ_p values. Moreover, the experimental emission and calculated LLTS energies indicated that the calculated values are systematically lower than those measured, in agreement with previous reports.

The most important correlation established was between the HOMO-LUMO energy gap, a very important characteristic that determines the applicability of compounds in photo- and electrochemical devices, and the σ_p values for the ligand substituents. In light-harvesting devices, the energy gap must overlap with the conduction band and the E_{LUMO} must be within or above the conduction band of a semiconductor, such as TiO_2. Our results demonstrate that by varying the substituents attached to the bipyridyl ring, the HOMO-LUMO gap and LUMO energy can be tuned. The correlations and insights presented here could help screen molecular candidates and rationally design improved optoelectronic photochemical and photocatalytic devices.

REFERENCES

REFERENCES

1 "Photophysical and Photochemical Properties of Ruthenium(II) Mixed-Ligand Complexes: Precursors to Homooligonuclear and Heterooligonuclear Complexes Containing Ruthenium(II), Platinum(II), Rhenium(I) and Rhodium(III)" D. P. Rillema and H. B. Ross, "The Seventh International Symposium on the Photochemistry and Photophysics of Coordination Compounds," Springer-Verlag, NY, **1987**, 151.

2 "A Rhenium(I) Bipyrimidine Tricarbonyl Complex Containing Methyl Viologen as the Sixth Ligand: NMR and Structural Results," L. N. Winslow, D. P. Rillema, J. H. Welch and P. Singh *Inorg. Chem.* **1989**, *28*, 1596

3 "Excited State Properties of Platinum(II) Complexes Containing Biphenyl as a Ligand: Complexes of the Type (bph)PtL_2, where L = Monodentate or Saturated Bidentate Ligands," C. B. Blanton, Z. Murtaza, R. Shaver and D. P. Rillema *Inorg. Chem*. **1992**, *31*, 3230.

4 "Hydrogel Immobilization of Tris(2,2'-Bipyridyl)Ruthenium(II) and Methyl Viologen at an Electrode Surface: Electrochemistry and Photocurrents," S. C. Perine, A. L. Crumbliss, A. K. Edwards and D. P. Rillema, The 197th National ACS Meeting, Dallas, Texas, April, 1989.

5 Hansch, C.; Leo, A.; Taft, R. W. *Chem. Rev.* **1991**, 91, 165-195.

6 Hammett, L. P. *J. Am. Chem. Soc*. **1937**, 59, 96-103.

7 Maestri, M.; Sandrini, D.; Balzani, V.; von Zelewsky, A.; Cornioley-Deuschel, C; Jolliet, P. *Helv. Chim. Acta* **1988**, *71*, 1053-1059.

8 Blanton, C. B.; Murtaza, Z.; Shaver, R. J.; Rillema, D. P. *Inorg. Chem.* **1992**, *31*, 3230-3235.

9 Blanton, C. B.; Rillema, D. P. *Inorg. Chim. Acta* **1990**, *168*, 145-147.

10 S. R. Stoyanov, J. M. Villegas, A. J. Cruz, L. L. Lockyear, J. H. Reibenspies and D. P. Rillema, *J. Chem. Theory Comput.*, 2005, **1**, 95-106.

11 C. Karakus, L. H. Fischer, S. Schmeding, J. Hummel, N. Risch, M. Schäferling and E. Holder, *Dalton Trans.*, 2012, **41**, 9623−9632.

12 N. Simhai, C. N. Iverson, B. L. Edelback and W. D. Jones, *Organometallics*, 2001, **20**, 2759-2766.

REFERENCES (continued)

13 Chen, Y.; Woods, C.; Perkovic, M. W.; Rillema, D. P. *J. Chem. Cryst*. **1996**, *26*, 527-531.

14 Zheng, G. Y.; Rillema, D. P. *Inorg. Chem*. **1998**, *37*, 1392-1397.

15 Chen. Y.; Merkert, J. W.; Murtaza, Z.; Woods, C.; Rillema, D. P. *Inorg. Chim. Acta* **1995**, 41-47.

16 Cornioley-Deuschel, C.; von Zelewsky, A. *Inorg. Chem*. **1987**, *26*, 3354-3358.

17 Kauffman, George B. ; Cowan, Dwaine O. "Cis - AND Trans – Dichlorobis (diethylsulfide) Platinum (II)" Inorganic Synthesis: 211-215.

18 (*a*) Bruker APEX2 User Manual, 2006, Bruker AXS Inc., Madison, Wisconsin, USA; (*b*) G. M. Schdrick, SHELXS97 and SHELXL97, 1997, University of Gottingen, Germany

19 D. P. Rillema, A. J. Cruz, C. Moore, K. Siam, A. Jehan, D. Base, T. Nguyen and W. Huang, *Inorg. Chem.*, 2012, **52**, 596-607.

20 D. Escudero and W. Thiel, *Inorg. Chem.* 2014, **53**, 11015–11019.

21 H. R. Zhekova, M. Seth and T. Ziegler, *Int. J. Quantum Chem.*, 2014, **114**, 1019−1029.

22 D. P. Rillema, J. K. Nagle, L. F. Barringer, Jr. and T. J. Meyer, *J. Am. Chem. Soc*., 1981, **103**, 56-62.

23 J. M. Villegas, S. R. Stoyanov and D. P. Rillema, *Inorg. Chem.*, 2002, **41**, 6688-6694.

24 G. Zhang and C. B. Musgrave, *J. Phys. Chem. A*, 2007, **111**, 1554-1561.

APPEDICES

APPENDICES

A. SOLVENT DEPENDENCY (SOLVATOCHROISM) OF COMPOUNDS

The platinum biphenyl compounds absorbance spectra show a solvent dependency in the visible region. In other words, the color of light of the solution is different depending on the solvent. This occurs because the absorption of light is an electronic transition, and when the solvent has a dielectric constant, the color absorbed will be different. This phenomenon is known as solvatochromism. An example is shown in Figure 5.1 for the platinum complex with an unsubstituted bipyridine.

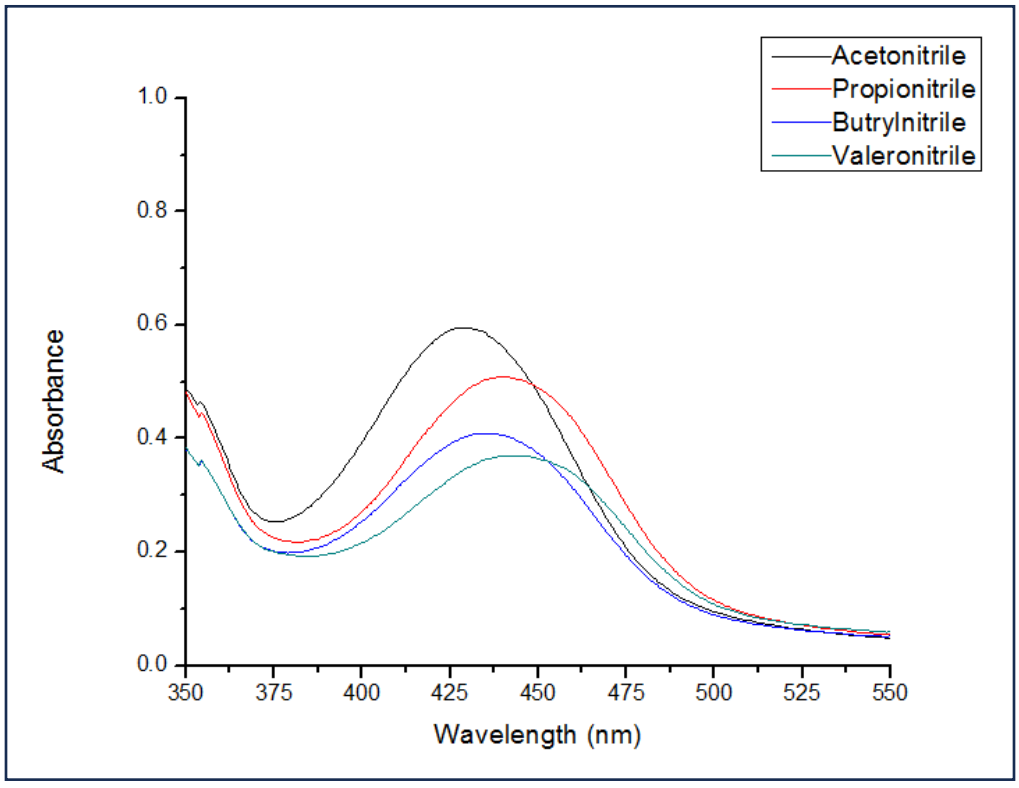

Figure A.1 Absorption of Pt(bph)(4,4'-Me_2-bpy) in various solvents

This behavior can be further explained by looking at the energy level diagram for the

transition from ground state to excited state as solvent polarity changes. As can be seen in figure x, as the polarity of the solvent increases, both the ground state and excited states are lowered in energy. This is due to the fact that the compounds have dipole moments (both in the ground and excited states), and as polarity increases, these states become more stabilized. The overall effect is the energy required for this transition is lowered, resulting in higher wavelentgths with increassing solvent polarity.

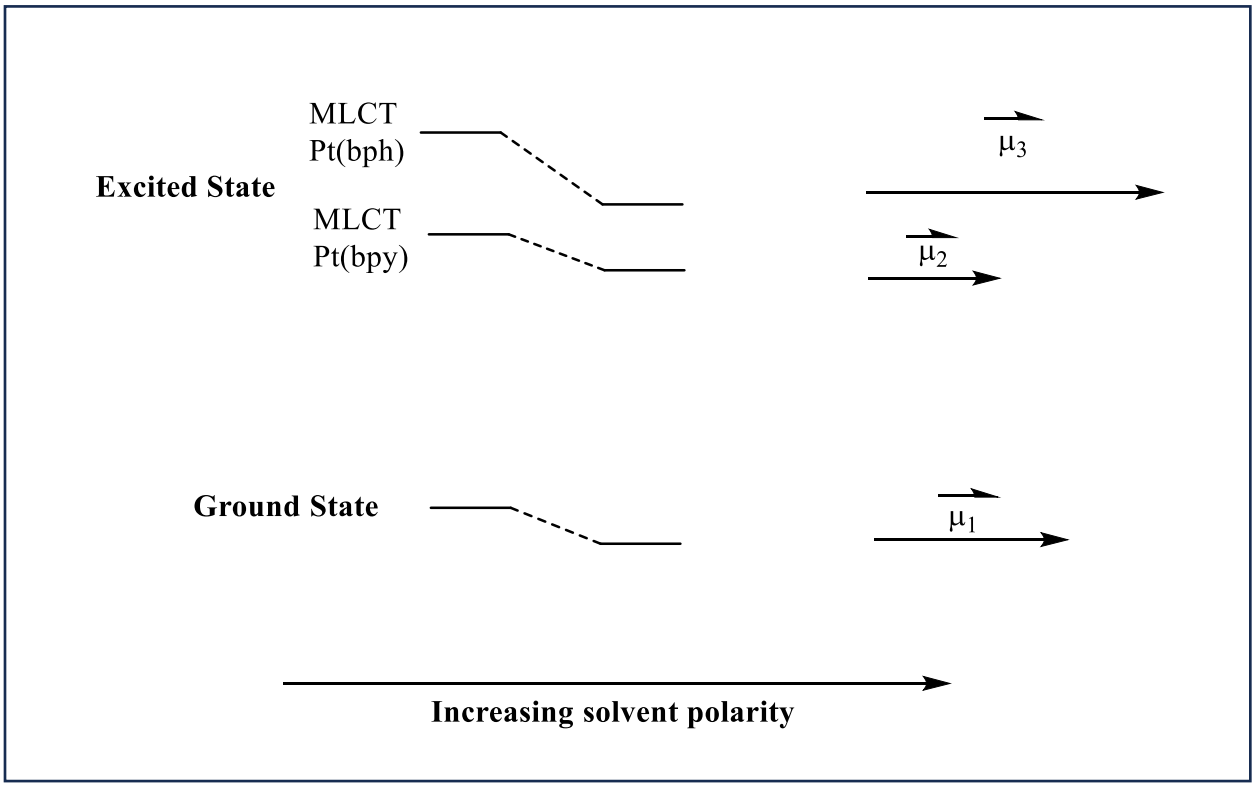

Figure A.2 Scheme illustrating MLCT energy changes based on solvent polarity

B. ALI JEHAN'S CO-AUTHORED POSTERS AND PUBLICATIONS

Posters

1. "Free Energy Correlations of Platinum(II) Biphenyl Complexes Containing 2,2'-Bipyridine Derivatives," D. P. Rillema, W. Huang, A. J. Cruz, K. Siam, D. Base and A. Jehan, The 243rd National American Chemical Society Meeting, San Diego, CA, March 2012.

2. "Electronic Properties of Platinum(II) Biphenyl Complexes Containing the Ligands 2,2'-Bipyridine and 1,10-Phenanthroline," D. Paul Rillema, Arvin John Cruz, Curtis E. Moore, Khamis Siam, Ali Jehan and Wei Huang, The 47th Midwest Regional Meeting of the American Chemical Society, Omaha, NE, October, 2012.

3. "Linear Free Energy Relationships in Platinum(II) Biphenyl Heterocyclic Ligand Complexes," D. Paul Rillema, Khamis Siam, Arvin Cruz, Curtis Moore, Ali Jehan, Venugopal Komreddy and Wei Huang, International Conference on Photochemistry, Leuven, Belgium, July, 2013.

4. "Dye Sensitized Solar Photoelectrochemical Cells," D. Paul Rillema, V. Komreddy, A. Jehan and H. Nguyen, The 246th National American Chemical Society Meeting, Indianapolis, IN, September, 2013.

5. "Substituent Effects in Platinum(II) Biphenyl Bipyridine Complexes," Ali Jehan, D, Paul Rillema, Khamis Siam, Arvin Cruz, Curtis Moore, Venugopal Komreddy and Huy Nguyen, The 247th National American Chemical Society Meeting, Dallas, TX, March, 2014.

6. "Preparation and characterization of a series of platinum(II) biphenyl complexes containing bipyridine ligands with substituents in the 4,4'-position," D. P. Rillema, A. Jehan, H. Nguyen, A. J. Cruz, C. Moore, 54th Midwest Regional Meeting of the American Chemical Society, Wichita, KS, October, 2019.

7. "Substituent Effects on the HOMO-LUMO Absorption and Emission of Pt(II)-Biphenyl Complexes containing 1,10-Phenanthroline Derivatives, A.J. Cruz, D.P. Rillema, S.R. Stoyanov, A. Jehan and K.S. Siam, 54th Midwest Regional Meeting of the American Chemical Society, Wichita, KS, October, 2019.

Publications

1. ‘‘Electronic, and Photophysical Properties of Platinum(II) Biphenyl Complexes Containing the 2,2’-Bipyridine and 1,10-Phenanthroline Ligands” D. P. Rillema, A. J. Cruz, C. Moore, K. Siam, A. Jehan, D. Base, T. Nguyen and W. Huang, *Inorg. Chem*. **2013** *52*, 596-607. DOI 10.1021/ic301393e.

2. “HOMO-LUMO Energy Gap Control in Platinum(II) Biphenyl Complexes Containing 2,2’-ipyridine Ligands” D. P. Rillema, S. R, Stoyanov, A. Cruz, H. Nguyen, C. Moore, W. Huang, K. Siam, A. Jehan and V. KomReddy, *Dalton Trans*. **2015**, *44*, 17075-17090 DOI: 10.1039/c5dt01891a.

3. “Bis(μ-diethyl sulfide – κ^2 S:S)bis[(biphenyl-2,2'-diyl)-platinum(II)]” D. P. Rillema, C. Moore and A. Jehan, *IUCrData* **2016** *1*, x160789.

4. “(Biphenyl-2,2’-diyl)[1,3-bis(diphenylphosphanyl)propane-κ^2*P,P’*]platinum(II)”D.P. Rillema, Curtis Moore and Ali Jehan, *IUCrData* **2016** *1*, x161277.